Wear 484-485 (2021) 204020

Contents lists available at ScienceDirect

Wear

journal homepage: www.elsevier.com/locate/wear

Bio-based ionic liquid crystal for stainless steel-sapphire high temperature ultralow friction

M.D. Avilés, F.J. Carrión, J. Sanes, M.D. Bermúdez *

Grupo de Ciencia de Materiales e Ingeniería Metalúrgica, Universidad Politécnica de Cartagena, 30202, Cartagena, Spain

ARTICLE INFO

Keywords:
Sliding friction
Lubricated wear
Steel
Sapphire
Ionic liquid crystal
Temperature

ABSTRACT

In the present work, the biobased protic ionic liquid crystal bis(2-hydroxyethyl) ammonium palmitate (DPA) has been studied as neat lubricant under linear reciprocating sliding at 75 °C, in the liquid crystalline region, and at 110 °C, above its melting point. Three different tribopairs have been studied using AISI 52100 steel, AISI 316L stainless steel and sapphire balls against AISI 316L disks. Tribological results at 75 °C are in agreement with the different sliding pairs and contact conditions. At 110 °C, a sharp friction coefficient reduction to reach an ultralow steady state value of 0.007–0.009, is observed for the sapphire-AISI 316L contact. Wear rate is also reduced in one order of magnitude. Results are related to water content in DPA, as determined by TG-MS. Wear mechanism are discussed upon the basis of optical and scanning electron microscopy (SEM/EDX) and of surface analysis by XPS.

1. Introduction

The reduction of energy loss due to friction and materials failure caused by wear are currently major technological and economic issues that need to be solved [1,2].

Ionic liquids (ILs) [3–17] have been studied as lubricants, lubricant additives and coatings to achieve friction and wear reduction. Tribological tests are usually carried out at ambient conditions, but for a growing number of sliding applications, they should withstand increasingly severe conditions. Very recently, the use of ionic liquids in an environment similar to that used in space lubrication have been described [14], and new functionalities of IL lubricants are being explored [15].

Environmentally benign, sustainable lubricants, including fatty acids and their derivatives [16–36], are currently being developed. In particular, bio-based protic ammonium carboxylate ionic liquids (PILs) [16,17,21,25–36] are a more ecofriendly alternative to conventional ILs composed of inorganic or heteroatom containing organic anions and heterocyclic cations.

PILs have been used both as neat lubricants [25–32] and as additives in aqueous or mineral [33–35] lubricants. Short alkyl chain ammonium carboxylate PILs [26–29] can be used as neat liquid lubricants at room temperature, while long alkyl chain PILs are solid at room temperature, as melting points increase with increasing alkyl chain length. This is the case of bis(2-hydroxyethyl)ammonium palmitate (DPA) [21].

DPA has been studied as lubricant additive both in water [32–35] and in a short alkyl chain PIL [36]. We have recently described the lubricant behavior of DPA as additive in water at room temperature and at 37 °C [34,35]. The results have opened up its potential for biocompatible applications.

There is a need for environmentally friendly lubricants under higher temperatures and contact pressures. However, the studies on environmentally friendly ionic liquid lubricants at high temperature are still scarce [37–39].

DPA is an ionic liquid crystal [40] i.e., a ionic liquid with transitions to mesomorphic phases. DPA presents two transition temperatures: from crystalline solid to liquid crystalline mesophase at 42.1°C, and the melting point to isotropic liquid at 105.2 °C [21].

DPA viscosity variations with temperature and shear rate have been recently described [21,34,35], in particular its non-Newtonian behavior at different temperatures, including those selected for the present study [34,35]. At 75 °C, in the liquid crystalline state, molecular interactions in the mesogenic structures determine the shear flow resistance, and a continuous viscosity decrease is observed under increasing shear rates, while at 110 °C, over its melting point, DPA is an isotropic fluid and viscosity reaches asymptotic constant values for shear rates higher than 150 s^{-1}. The thermal transitions from crystalline solid to liquid crystal and from liquid crystalline phase to isotropic liquid induce structural

* Corresponding author.
E-mail address: mdolores.bermudez@upct.es (M.D. Bermúdez).

https://doi.org/10.1016/j.wear.2021.204020
Received 5 March 2021; Received in revised form 28 June 2021; Accepted 5 July 2021
Available online 9 July 2021

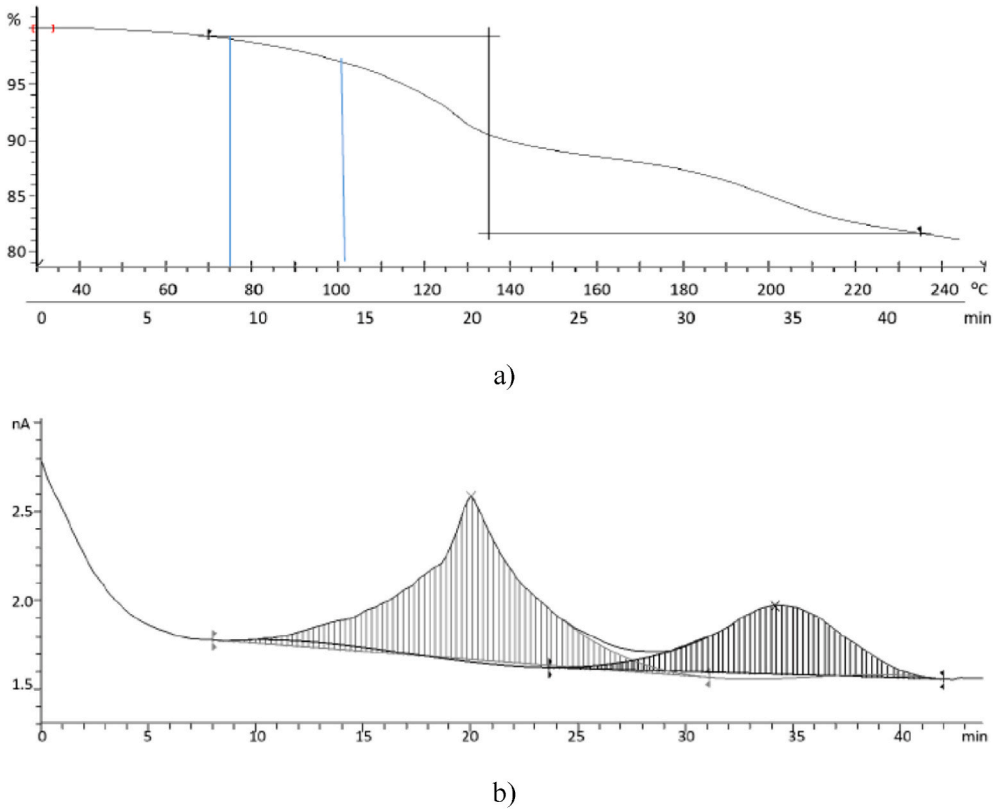

Fig. 1. TG-MS for DPA: a) Weight percentage vs temperature and time; b) Ion current vs time with integration of $m/z = 18$ peaks.

changes which could have a pronounced influence in the tribological results when DPA is used as neat lubricant.

Thus, in the present work, DPA has been used as neat lubricant under linear reciprocating sliding tests at high temperature using AISI 52100, AISI 316L and sapphire balls, against AISI 316L disks.

PILs that contain –NH groups and –OH substituents, such as is the case of the hydroxyethylammonium cations present in DPA, form hydrogen bonds and are strongly hydrophilic. This highly hydrophilic nature increases their water absorption capability [41].

Under the experimental conditions used in the present work, below and above 100 °C, the tribological results could be also determined by water contents, thus thermogravimetric-mass spectrometry studies have been carried out in order to measure water percentages present in the ionic liquid crystal lubricant.

DPA has been previously described as lubricant and lubricant additive at room temperature. The main aims of the present research are to establish the feasibility of using this renewable source lubricant under conditions close to those of a broader range of practical applications, and to study surface interactions and wear mechanisms for both steel-steel and ceramic-steel contacts.

2. Experimental

Synthesis and characterization of DPA have been previously described [21]. Thermogravimetric mass spectrometry analysis (TG-MS), was performed using a TGA/DSC 1HT (Mettler-Toledo) with a Thermostar, QMS 300M3 quadrupole mass spectrometer (Balzers), heating from 30 to 350 °C at a heating rate of 5 °C/min in a N_2 atmosphere with a flow of 50 mL/min. Samples (8.8 mg) were placed in closed perforated aluminium pans.

Calibration with calcium oxalate monohydrate ($CaC_2O_4{\cdot}H_2O$; Alpha Aesar; 99.99% purity) was carried out before water determination in DPA. Water loss from calcium oxalate monohydrate takes place on the temperature range from 100 to 240 °C. During this interval, ion current for $m/z = 18$, corresponding to loss of water, increases. Integration of the curve allows the calculation of the ratio between mass of water (mg) and variation of ion current with time ($nA{\cdot}s^{-1}$).

Tribological tests were carried out using a tribometer (Anton Paar, Switzerland) at the reciprocating configuration (sliding frequency of 2 Hz; sliding distance 175 m, amplitude 5 mm), under a normal load of 1 N. Steel-steel and steel-ceramic contacts were selected as counterparts, as these materials are used in tribological applications both at room temperature and at high temperature.

AISI 316L disks (25 mm diameter; 5 mm thick; Ra $<$ 0.15 μm) were used against three different ball materials: AISI 52100 steel [1.6 mm diameter; contact pressure: 1.03 GPa (average); 1.55 GPa (maximum)]; AISI 316L stainless steel [1.6 mm diameter; contact pressure: 1.01 GPa (average); 1.51 GPa (maximum)] and sapphire [1.5 mm diameter: 1.30 GPa (average); 1.95 GPa (maximum)]. Hertzian contact pressures were calculated from Young's modulus and Poisson's ratio values [42]. Before each test, the surface of the AISI 316L disk was covered with 5 mg of DPA.

Tribological tests were performed at 75 °C (in the mesomorphic region) and at 110 °C (in the isotropic liquid state). All tribological tests were repeated at least three times in order to ensure reproducibility.

Surfaces were cleaned with *n*-hexane and dried in hot air, before and after each test. Wear rates, calculated [43] from volume loss measurements, were determined with an optical profiler (Talysurf CLI). Element maps were obtained by means of SEM micrographs and EDX, using a Hitachi S3500 N. XPS analysis was obtained with a K-Alpha Thermo-Scientific equipment, with 0.1 eV precision for binding energy values; thickness of the analyzed surface layer: 3–5 nm. AISI 316L disk surface was analyzed before the tests, as a reference.

Table 1
Friction coefficient and wear rate variation with temperature and ball material.

75 °C		
Ball material	COF	Wear rate ($mm^3/N{\cdot}m$)
AISI 52100	0.201 (±0.005)	$(4.12 \pm 0.55){\cdot}10^{-4}$
AISI 316L	0.078 (±0.004)	$(5.68 \pm 0.22){\cdot}10^{-7}$
Sapphire	0.100 (±0.009)	$(1.19 \pm 0.47){\cdot}10^{-5}$
	110 °C	
AISI 52100	0.212 (±0.011)	$(4.94 \pm 0.19){\cdot}10^{-4}$
AISI 316L	0.091 (±0.003)	$(1.71 \pm 0.11){\cdot}10^{-5}$
Sapphire	0.015 (±0.002)	$(3.05 \pm 0.14){\cdot}10^{-5}$

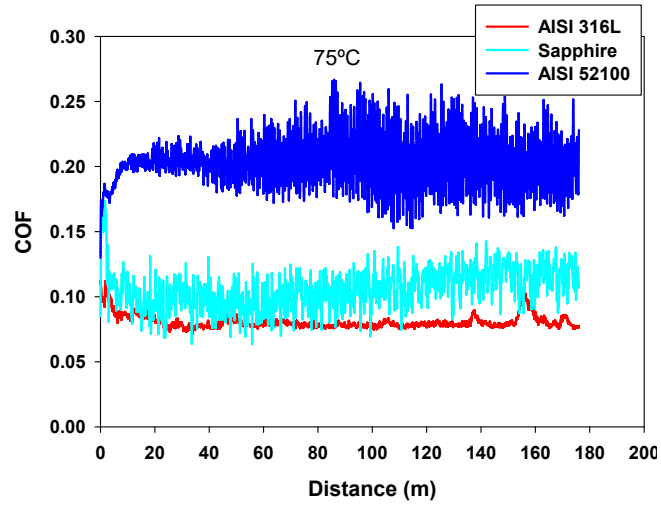

b)

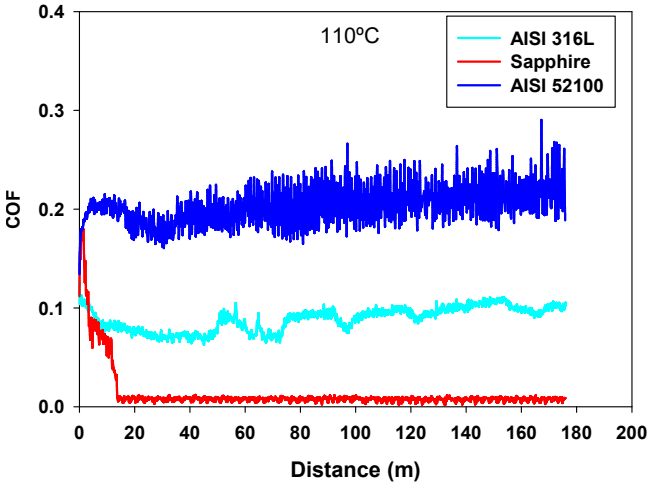

Fig. 2. Coefficient of friction vs sliding distance: a) 75 °C; b) 110 °C.

3. Results and discussion

3.1. Thermal stability and water loss

The complete TGA thermogram and degradation temperatures of DPA has been recently reported [34]. TGA thermogram in Fig. 1a shows that DPA presents two water loss steps, a first weight loss step between 70 and 135 °C assignable to absorbed water (as determined by mass spectroscopy, from $m/z = 18$; Fig. 1b).

This absorbed water accounts for a 5.46 wt %, calculated as the integration under the first curve (Fig. 1b). Tribological tests at 75 and 110 °C are therefore within this first water loss region and before the second weight loss step. This second weight loss step, in the range 170–240 °C (Fig. 1a), also corresponds to loss of H_2O (2.76 wt %, from the integration of the second peak in Fig. 1b), and could be assigned to thermal degradation of DPA.

3.2. Tribological results

In order to study the influence of temperature on the tribological performance of the ionic liquid crystal DPA, preliminary variable temperature tests were programed for sapphire-stainless steel, heating from 60 °C (when DPA is in the liquid crystalline state) to 110 °C (just over DPA melting point) under a constant temperature rate of 2 °C/min. The results showed that friction coefficient decreases from 0.17 to 0.08, between 60 °C and 75 °C. From 75 °C to 110 °C, friction coefficient values around 0.08–0.10 are maintained. These results confirm the reduction of friction coefficient with increasing temperature for DPA within its liquid crystalline range. The lower friction coefficient values for the 75 to 110 °C interval could be associated to water evaporation, as we have seen in Fig. 1. However, no transition to ultralow friction values as those previously described at room temperature for a protic ammonium succinate ionic liquid [26] are observed. This is attributed to the severe wear experienced by the stainless steel disk during the high friction period, from 60 °C to 75 °C.

In view of these preliminary results, 75 and 110 °C were selected for constant temperature tests for sapphire-stainless steel and also for stainless steel against itself or against 52100 steel.

Table 1 shows the tribological results for each temperature and sliding pair. At 75 °C, the order of friction coefficients and wear rates for stainless steel disk as a function of ball material is: AISI 52100 ball > Sapphire ball > AISI 316L ball. However, at 110 °C, the order changes to: AISI 52100 ball > AISI 316L ball > Sapphire ball.

It is worth noting that while steel-steel contacts show the expected friction coefficient and wear rate increase with temperature increase, the corresponding values for sapphire-AISI 316L decrease when temperature increases. Particularly relevant is the reduction in the average friction coefficient, from 0.10 at 75 °C to 0.015 at 110 °C.

Representative friction coefficient-sliding distance records for all materials at 75 °C and 110 °C are shown in Fig. 2a and b, respectively. At 75 °C, a smooth friction coefficient variation with distance is only observed for AISI 316L against itself, in agreement with lower average friction and wear rate values. At 110 °C, friction records for steel-steel pairs are similar to those recorded at 75 °C. For sapphire-stainless steel, initial running-in friction record is similar to that observed at 75 °C, but an immediate friction drop quickly leads to steady-state values of 0.007–0.009 from 20 m to the end of the test.

Running-in friction coefficient values are very high (0.17) as correspond to the severe contact conditions. At both temperatures, friction drops rapidly below 0.10. At 75 °C this value is then maintained along the entire sliding distance. In contrast, at 110 °C, the sharp reduction of friction coefficient is maintained until an ultralow steady-state friction value of 0.007–0.009 is reached, approximately after 20 m.

Superlubricity [44] in sapphire sliding against itself under lubrication with a solution of phosphoric acid in water, at room temperature, has been recently described [45]. Friction coefficient evolution with sliding distance were similar to those described in the present work at 110 °C (Fig. 2b), with a high friction running-in period. Friction decrease and transition to superlubricity was associated with water evaporation during the running-in period and formation of an adsorbed thin film which forms a hydrogen bonding network with the surfaces.

We have seen (Fig. 1) that DPA is losing absorbed water between 70 and 135 °C. This water evaporation could contribute to the ultralow friction coefficient observed at 110 °C, when formation of an efficient DPA boundary layer is more favored than at the lower temperature of

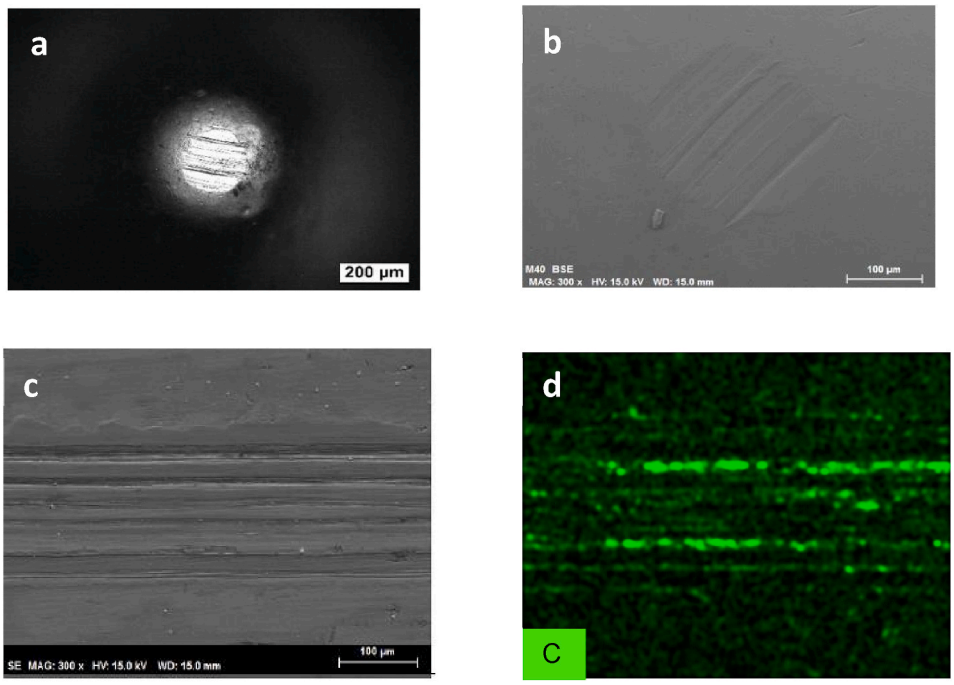

Fig. 3. AISI 316L-AISI 316L at 75 °C: a) Optical micrograph and b) SEM micrograph of AISI 316L ball; c) SEM micrograph of the wear track on AISI 316L disk; d) Carbon element map on wear track shown in c).

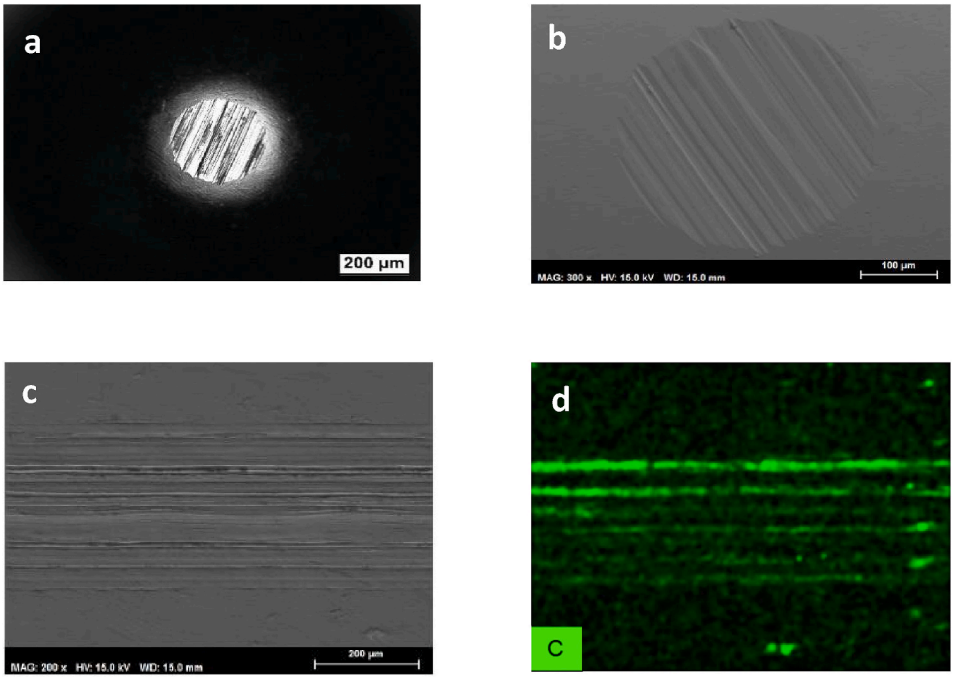

Fig. 4. AISI 316L-AISI 316L at 110 °C: a) Optical micrograph and b) SEM micrograph of AISI 316L ball; c) SEM micrograph of the wear track on AISI 316L disk; d) Carbon element map on wear track shown in c).

75 °C, closer to the water evaporation onset.

3.3. Surface analysis

Sapphire and steel balls and stainless steel disks surfaces were examined after the tests in order to determine the main wear and surface damage mechanisms. Figs. 3 and 4 show wear tracks on AISI316L ball and AISI316L disk after the tests at 75 °C (Fig. 3a–d) and 110 °C (Fig. 4a–d).

Optical and SEM micrographs of the ball surface (Fig. 3a–c and 4a-4c) show parallel abrasion marks, in correspondence with the parallel grooves present on the disk (Figs. 3c and 4c). EDX carbon maps (Figs. 3d and 4d) show a higher carbon (in green) content inside the deep abrasion grooves, assigned to DPA lubricant tribolayer.

Fig. 4a–d shows that the abrasive mechanism we have seen for the AISI 316L-AISI 316L contact becomes more severe when temperature is raised to 110 °C. Both optical (Fig. 4a) and electron (Fig. 4b) micrographs of the ball show that the severe abrasion has produced a large flat

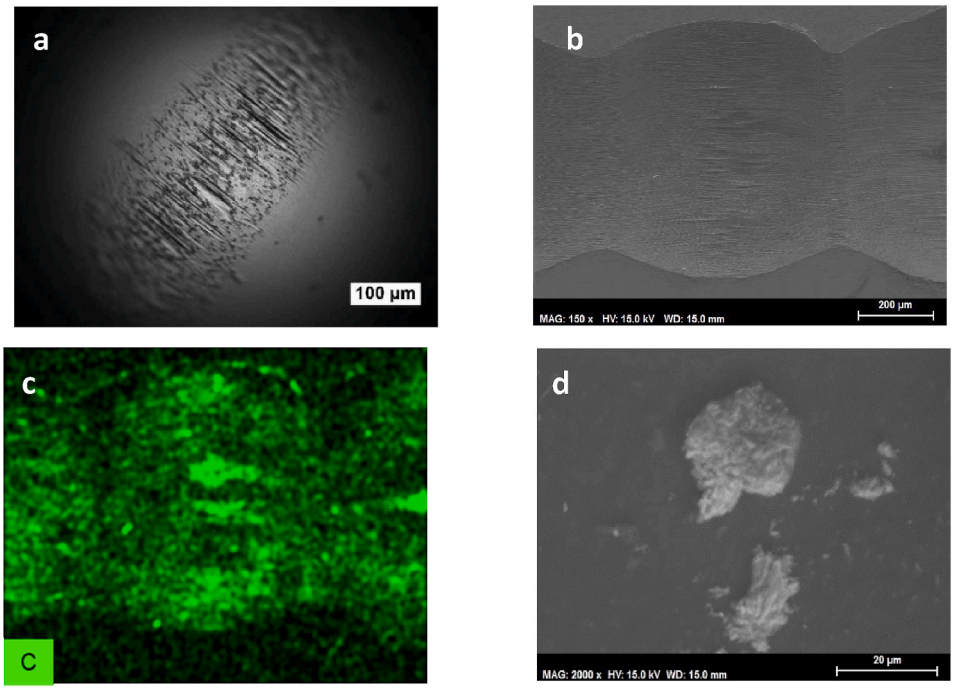

Fig. 5. AISI 52100-AISI 316L at 75 °C: a) AISI 52100 ball; b) Wear track on AISI 316L disk; c) Carbon element map on the wear track shown in b); d) Wear debris from AISI 316L disk.

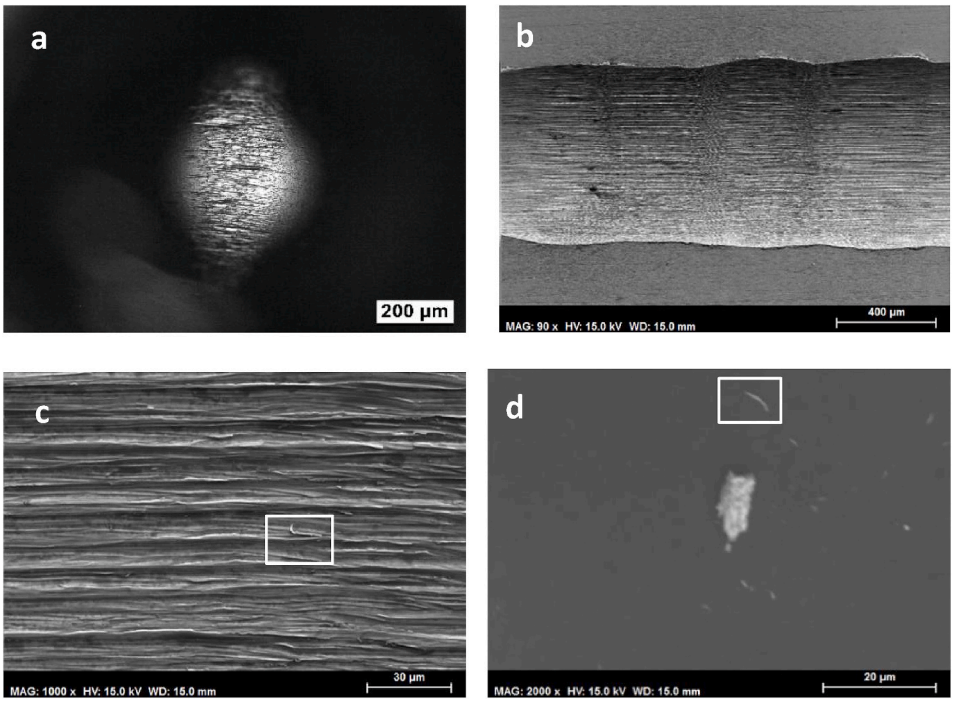

Fig. 6. AISI 52100-AISI 316L at 110 °C: a) Optical micrograph of AISI 52100 ball; b) SEM micrograph of wear track on AISI 316L disk; c) Magnification of b) with detail showing wear debris chip removal; d) Wear debris aggregate and detail showing chip morphology.

circular scar.

AISI 52100 ball (Fig. 5a) shows deep abrasion grooves after the test against AISI 316L disk at 75 °C, without the changes in spherical geometry observed for AISI 316L ball (Fig. 4a). As expected, the substitution of AISI 316L ball by the AISI 52100 increases the severity of surface damage on AISI 316L disk (Fig. 5b and c). The wear track presents some abrasion marks but, in this case, the main mechanism is adhesive wear. A marked stick-slip effect is also present as evidenced by the periodic variation in wear track width (Fig. 5b). EDX element map (Fig. 5c) shows the presence of carbon inside the wear track.

In this case, the severity of the contact conditions produces the loss of wear debris (Fig. 5d), including large particles formed by adhesion of more finely divided ones, as is characteristic of steel adhesive wear.

When heated at 110 °C, the severity of the AISI 52100-AISI 316L contact further increases, giving rise to an abrasive mechanism (Fig. 6a-c), clearly illustrated in the magnification of the wear track surface on

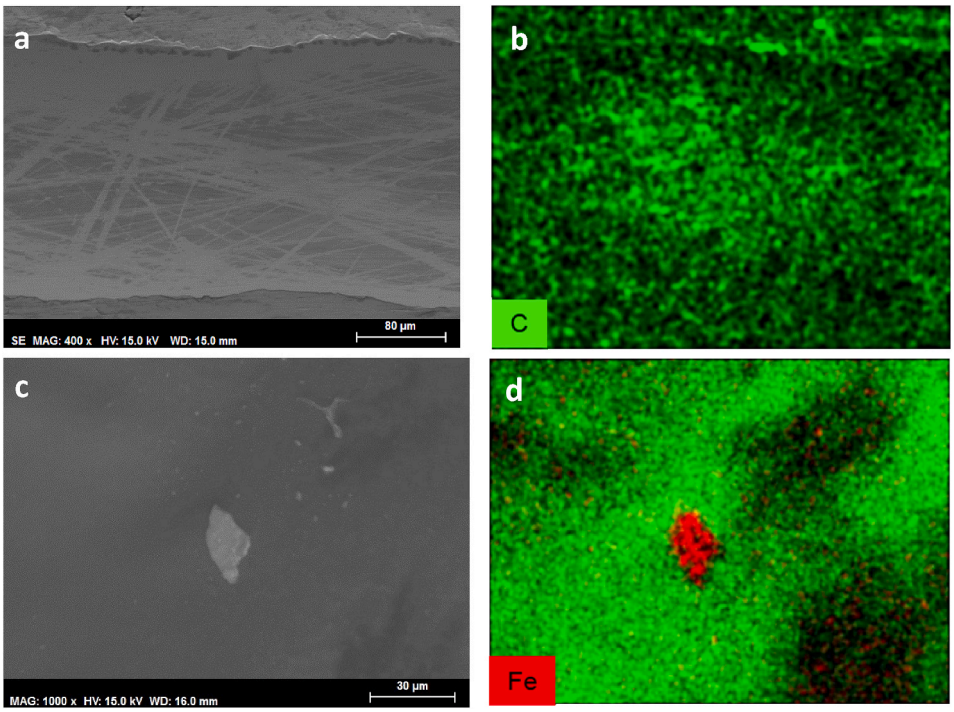

Fig. 7. Sapphire-AISI 316L at 75 °C: a) SEM micrograph of the wear track; b) Carbon element map; c) SEM micrograph of wear debris; d) Iron element map of wear debris.

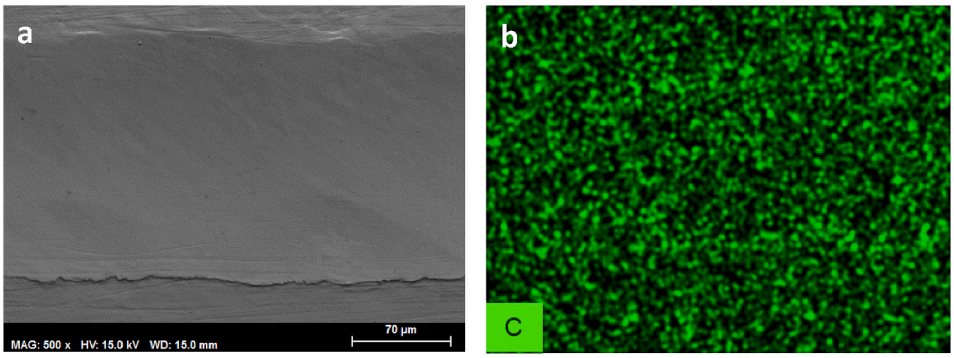

Fig. 8. Sapphire-AISI 316L at 110 °C: a) SEM micrograph of the wear track on AISI 316L disk; b) Carbon element map.

AISI 316L shown in Fig. 6c. A machining chip removal mechanism can also be observed (see details in Fig. 6c and d). In agreement with this mechanism, wear debris are not only the result of particle adhesion, but also show a chip morphology.

As expected, sapphire balls show no surface damage after the tribological tests against AISI 316L disk. Wear track on the steel disk at 75 °C (Fig. 7a) shows an adhesive mechanism, with the presence of carbon uniformly distributed, mainly at the bottom of the track and on the edge (Fig. 7b). Some wear debris are also removed from the steel surface (Fig. 7c and d).

At 110 °C lubrication with DPA of the sapphire-AISI 316L contact produces a mild adhesive wear, with a wear track (Fig. 8a) free from abrasion marks and also free from the high carbon concentration (Fig. 8b) observed for steel-steel contacts. No wear debris are recovered in this case. These observations are in agreement with friction coefficient and wear rate values shown in Table 1 and confirm the best performance of DPA lubricant at 110 °C for sapphire-AISI 316L contact.

XPS surface analysis was used to determine the composition of the surface layer on the wear track on AISI 316L disk after the tests against AISI 52100 and sapphire balls at 110 °C, and the results are shown in Table 2.

AISI 316L disk XPS analysis before the test shows C1s peaks at 285.0 eV, 286.6 eV and 289.2 eV. Wear tracks show additional C1s peaks around 288 eV, assigned to C═O (see Table 2). O1s peaks for AISI 316L before the test (530.6 eV, 532.4 eV and 533.9 eV) are similar to those found inside the wear tracks. The additional 531.5 and 531.4 eV peaks (Table 2) are assigned to the presence of hydroxide groups. Fe 2p3/2 and Cr 2p3/2 peaks of the original disk are similar to those found after the tribological tests (Table 2).

The main differences in the composition of the wear scar surfaces between steel-steel and steel-sapphire (Table 2), are a decrease in total C1s atomic percentage, in agreement with EDX observations (Fig. 8b), and an increase in total O1s contents on stainless steel after the test against AISI 52100 steel.

A weak C1s peak at 289.2 eV (Table 2), which could be due to carboxylate anions, is only present after the test against sapphire.

O1s peaks for sapphire-steel at 531, 532 and 534 eV can be assigned to metal oxides or hydroxides, carboxylate and carbonyl groups, respectively.

For steel-steel, high concentrations of the O1s signals at 530 and 531

Table 2
XPS surface analysis (binding energies and atomic percentages) inside the wear track on AISI 316L disk after the tests at 110 °C.

Element	AISI 52100 ball		Sapphire ball		Chemical state assignments
	Binding energy (eV)	Atomic %	Binding energy (eV)	Atomic %	
C1s	285.0	29.1	285.0	56.9	Aliphatic carbon
	286.2	10.5	286.3	16.6	C–O
	288.0	8.0	287.9	2.7	C=O
	–	–	289.2	2.2	COO^-
O1s	530.0	13.3	–	–	Metal oxides
	531.5	19.0	531.4	8.1	OH
	–	–	532.8	6.7	COO^-
	533.7	5.7	–	–	H_2O
	–	–	534.2	1.2	CO
N1s	400.0	1.0	400.0	1.8	HN–C
	401.3	0.2	401.4	0.4	N–C
Cr 2p3/2	574.1	0.5	–	–	Cr (0)
	575.9	1.8	575.2	0.2	Cr–CO
	577.1	1.9	577.4	1.0	Cr–OH
	578.5	0.7	578.8	0.7	Cr_2O_3
Ni 2p3/2	852.8	0.6	–	–	Ni(0)
	853.9	0.1	854.1	0.2	NiO
Fe 2p3/2	706.8	1.2	–	–	Fe (0)
	707.8	0.9	708.2	0.3	FeO
	710.4	4.3	709.3	0.3	Fe_2O_3
	–	–	711.8	0.6	FeO(OH)
	713.2	0.9	–	–	Fe^{2+} (satellite)
	–	–	714.3	0.1	Fe^{3+} (satellite)

eV, corresponding to oxides and hydroxides are found. In particular, the O1s peak found at 530 eV for the steel ball is assigned to iron oxide (FeO) [46].

A strong increase in atomic percentage for the O1s signal at 531.5 eV, corresponding to metal hydroxides, such as $Ni(OH)_2$ or $Cr(OH)_3$ is observed for the steel-steel case.

A new high O1s binding energy at 533.7 eV, with a high atomic concentration, which is assignable to adsorbed water, is not present inside the wear path for the sapphire ball. The fact that O1s binding energies assignable to CO and COO groups are only detected on the steel surface after sliding against sapphire could be attributed to a stronger surface interaction which could be responsible for the better tribological performance found in this case, and is in agreement with very recently described results [47] on fatty acid derived ILs composed of quaternary ammonium cations and carboxylate anions.

Two N1s signals are found in both cases. The most abundant peak, at 400 eV is assignable to the ammonium cation nitrogen, while the minor peak at 401 eV could be due to N–C [41] The presence of N1s peaks from the cation and the absence of binding energies assignable to the presence of Fe–N has been proposed as evidence of the physical interaction between protic ammonium carboxylate lubricants and iron surfaces [41].

The main Cr2p3/2 signal at 577 eV could be due to chromium hydroxide, while the minor signals at 575 and 579 eV are tentatively assigned to Cr–CO- and Cr_2O_3, respectively. The weak Cr (0) binding energy at 574 eV is only present in the steel-steel wear path.

A weak Ni2p3/2 peak at 854 eV, due to NiO, is found in both cases. Ni(0), at 853 eV, is only present in the steel-steel wear track.

Fe 2p3/2 at 708 eV, assignable to Fe_3O_4, is only observed inside the wear path for sapphire-steel, while Fe (0) binding energy, at 706 eV, is only found for steel-steel. Three signals between 708 and 712 eV, present in the stainless steel wear path after the test against sapphire, are assigned to FeO, Fe_2O_3 and FeO(OH), respectively. In steel-steel, the most abundant Fe 2p3/2 binding energy is that at 710.4 eV, due to the presence of iron oxides.

In steel-steel pairs, strong adhesion between steel pair materials and severe abrasion mechanisms cause lubricant failure. A similar mechanism occurs for sapphire-stainless steel at 75 °C, with the significant reduction of abrasion due to the absence of wear of the sapphire ball.

In contrast, for the sapphire-steel contact at 110 °C, the lubricant film is acting as friction and wear reducing. The higher contact pressure and the lower thermal conductivity of sapphire with respect to steel, could increase the temperature at the interface [48], thus further reducing water content in DPA. The above discussed XPS results are in agreement with a lower water content at the stainless steel surface after the test against sapphire at 110 °C.

Previous results for fatty acid PILCs at room temperature have shown that water evaporation increases friction and wear for sapphire-stainless steel pair due to precipitation of the solid at the interface. This solidification upon loss of water does not occur when the temperature is maintained above the melting point, thus an outstanding friction coefficient reduction is achieved.

4. Conclusions

A hydrophilic diprotic ammonium palmitate ionic liquid crystal has been studied as neat lubricant at high temperature in steel-steel and sapphire-steel reciprocating sliding conditions.

Two temperatures were selected for tribological tests, the first one above the transition from crystalline solid to liquid crystal mesophse, and the second one above the transition from liquid crystalline mesophase to isotropic liquid.

At 75 °C, when the lubricant is in the mesomorphic region, severe wear and high friction coefficients are found for all tribopairs.

At 110 °C, when the lubricant is in the isotropic liquid state, friction coefficients and wear rates increase for steel-steel. In contrast, for sapphire-stainless steel, 85% reduction in friction coefficient and 75% reduction in wear rate is observed with respect to values at 75 °C. The sharp friction coefficient reduction to 0.015 is only observed when a constant temperature of 110 °C has been reached before the sliding starts.

Wear mechanisms are severe abrasion for steel-steel pairs and mainly adhesive wear for sapphire-stainless steel. Surface analysis of the wear tracks show a higher concentration of metal oxides and hydroxides and adsorbed water on the surface of stainless steel after the test against AISI 52100 steel ball at 110 °C.

The protic ammonium palmitate ionic liquid is hydrophilic and presents two water loss steps, the first step in the temperature range selected for tribological tests, between 70 and 135 °C. The presence of water could favor tribocorrosion at the steel-steel interface, however, surface analysis indicates a physical rather than tribochemical interaction between the steel surface and the lubricant. The higher temperature at the contact asperities in the case of sapphire-stainless steel could contribute to remove a higher proportion of adsorbed water and to enhance the tribological performance of the lubricant. Surface analysis of the stainless steel wear track after sliding against sapphire at 110 °C, as compared with the same surface before the tribological tests, confirms the presence of functional groups from the lubricant, which could be responsible for the ultralow friction coefficient.

Author statement

M.D. Avilés: Investigation; Methodology; Software. F.J. Carrión: Funding acquisition; Methodology. J. Sanes: Funding acquisition; Supervision. M.D. Bermúdez: Funding acquisition; Supervision; Conceptualization; Writing

Declaration of competing interest

The authors declare that they have no known competing financial interests or personal relationships that could have appeared to influence the work reported in this paper.

Acknowledgments

This research was funded by Spanish Ministerio de Ciencia e

Innovación, Agencia Estatal de Investigación (AEI), and the European Union FEDER Program (Grant # MAT2017–85130-P). “Este trabajo es resultado de la actividad desarrollada en el marco del Programa de Ayudas a Grupos de Excelencia de la Región de Murcia, de la Fundación Seneca, Agencia de Ciencia y Tecnología de la Región de Murcia (Grant #19877/GERM/15)”.

References

[1] K. Holmberg, A. Erdemir, Influence of tribology on global energy consumption, costs and emissions, Friction 5 (2017) 263–284, https://doi.org/10.1007/s40544-017-0183-5.
[2] K. Holmberg, P. Kivikytö-Reponen, P. Härkisaari, K. Valtonen, A. Erdemir, Global energy consumption due to friction and wear in the mining industry, Tribol. Int. 115 (2017) 116–139, https://doi.org/10.1016/j.triboint.2017.05.010.
[3] K. Amzad, R. Gusain, M. Saha, O.P. Khatri, Fatty acids-derived protic ionic liquids as lubricant additive to synthetic lube base oil for enhancement of tribological properties, J. Mol. Liquids 293 (2019) 111444, https://doi.org/10.1016/j.molliq.2019.111444.
[4] R. Gusain, O.P. Khatri, Fatty acid ionic liquids as environmentally friendly lubricants for low friction and wear, RSC Advances 6 (2016) 3462–3469, https://doi.org/10.1039/C5RA25001C.
[5] A.Z. Syahir, N.W.M. Zulkitli, H.H. Masjuki, M.A. Kalam, A. Alabdulkarem, M. Gulzar, L.S. Khong, M.H. Harith, A review on bio-based lubricants and their applications, J. Cleaner Prod. 168 (2017) 997–1016, https://doi.org/10.1016/j.jclepro.2017.09.106.
[6] B. Khemchandani, A. Somers, R. Howlett, A.K. Jaiswal Ak, E. Sayanna, M. A. Forsyth, Biocompatible ionic liquid as an antiwear additive for biodegradable lubricants, Tribol. Int. 77 (2014) 171–177, https://doi.org/10.1016/j.triboint.2014.04.016.
[7] N. Rivera, A. García, A. Fernandez-Gonzalez, D. Blanco, R. Gonzalez, A. Hernandez Battez, Tribological behavior of three fatty acid ionic liquids in the lubrication of different material pairs, J. Mol. Liquids 296 (2019) 111858, https://doi.org/10.1016/j.molliq.2019.111858.
[8] M. Sernaglia, D. Blanco, A.H. Battez, R. Gonzalez, A. Fernandez-Gonzalez, M. Bartolome, Two fatty acid anion-based ionic liquids - part II: effectiveness as an additive to a polyol ester, J. Mol. Liq. 310 (2020), https://doi.org/10.1016/j.molliq.2019.111858 article number 113158.
[9] I. Minami, Ionic liquids in tribology, Molecules 14 (2009) 2286–2305, https://doi.org/10.3390/molecules14062286.
[10] M.D. Bermúdez, A.E. Jiménez, J. Sanes, F.J. Carrión, Ionic liquids as advanced lubricant fluids, Molecules 14 (2009) 2888–2908, https://doi.org/10.3390/molecules14062286.
[11] T. Torimoto, T. Tsuda, K. Okazaki, S. Kuwabata, New frontiers in materials science opened by ionic liquids, Adv. Mater. 22 (2010) 1196–1221, https://doi.org/10.1002/adma.200902184.
[12] A.E. Somers, P.C. Howlett, D.R. MacFarlane, M. Forsyth, A review of ionic liquid lubricants, Lubricants 1 (2013) 3–21, https://doi.org/10.3390/lubricants1010003.
[13] M.R. Cai, Q.L. Yu, W.M. Liu, Ionic liquid lubricants: when chemistry meets tribology, Chem. Soc. Rev. 49 (2020) 7753–7818, https://doi.org/10.1039/D0CS00126K.
[14] E. Nyberg, C. Schneidhofer, L. Pisarova, N. Dörr, I. Minami, Ionic liquids as performance ingredients in space lubricants, Molecules 2021 26 (2021) 1013, https://doi.org/10.3390/molecules26041013.
[15] C.B. Stump, Y. Zhou, H. Luo, N.D. Leonard, B.M. Viola, J. Qu, New functionality of ionic liquids as lubricant additives: mitigating rolling contact fatigue, ACS Appl. Mater. Interfaces 11 (2019) 30484–33049, https://doi.org/10.1021/acsami.9b10001.
[16] T.L. Greaves, C.J. Drummond, Protic ionic liquids: properties and applications, Chem, Rev 108 (2008) 206–237, https://doi.org/10.1021/cr068040u.
[17] T.L. Greaves, C.J. Drummond, Protic ionic liquids: evolving structure–property relationships and expanding applications, Chem. Rev. 115 (2015) 11379–11448, https://doi.org/10.1021/acs.chemrev.5b00158.
[18] S.A.S. Amiril, E.A. Rahim, S. Syahrullail, A review on ionic liquids as sustainable lubricants in manufacturing and engineering: recent research, performance and applications, J. Clean. Prod. 168 (2017) 1571–1589, https://doi.org/10.1016/j.jclepro.2017.03.197.
[19] Y. He, H. Li, C. Qu, W. Cao, M. Ma, Recent understanding of solid-liquid friction in ionic liquids, Green Chem. Eng (2021), https://doi.org/10.1016/j.gce.2020.10.006 in press.
[20] N. Nasirpour, M. Mohammadpourfard, S.Z. Heris, Ionic liquids: promising compounds for sustainable chemical processes and applications, Chem. Eng. Res. Design 160 (2020) 264–300, https://doi.org/10.1016/j.cherd.2020.06.006.
[21] A.A.C. Toledo, G.J. Maximo, M.C. Costa, R.L. Cunha, J.F.B. Pereira, K.A. Kurnia, E. A.C. Batista, A.J.A. Meirelles, Phase behavior and physical properties of new biobased ionic liquid crystals, J. Phys. Chem. B 121 (2017) 3177–3189, https://doi.org/10.1021/acs.jpcb.7b01384.
[22] M.J. Fan, L. Ma, C.Y. Zhang, Z.J. Wang, J.C. Ruan, M. Han, Y.Y. Ren, C. Zhang, D. S. Yang, F. Zhou, W.M. Liu, Bio-based green lubricants: physicochemical, tribological and toxicological properties of fatty acid ionic liquids, Tribol. Trans. 61 (2018) 195–206, https://doi.org/10.1080/10402004.2017.1290856.
[23] A. Khan, R. Gusain, M. Sahai, O. Khatri, Fatty acids-derived protic ionic liquids as lubricant additive to synthetic lube base oil for enhancement of tribological properties, J. Mol. Liq. 293 (2019) 111444, https://doi.org/10.1016/j.molliq.2019.111444.
[24] J.L. Viesca, J. Faes, N. Rivera, M. Cadenas, R. González, Thermal stability, traction and tribofilm formation of three fatty acid-derived ionic liquids, Tribol. Int. 154 (2021), https://doi.org/10.1016/j.triboint.2020.106712. Article number 106712.
[25] Y.J. Shi, R. Larsson, Non-corrosive and biomaterials protic ionic liquids with high lubricating performance, Tribol. Lett. 63 (2016) 1, https://doi.org/10.1007/s11249.016.0692.9.
[26] T. Espinosa, M. Jiménez, J. Sanes, M.D. Bermúdez, Ultra-low friction with a protic ionic liquid boundary film at the water-lubricated sapphire-stainless steel interface, Tribol. Lett. 53 (2014) 1–9, https://doi.org/10.1007/s11249.013.0238.3.
[27] M.D. Avilés, F.J. Carrión-Vilches, J. Sanes, M.D. Bermúdez, Diprotic ammonium succinate ionic liquid in thin film aqueous lubrication and in graphene nanolubricant, Tribol. Lett. 67 (2019) 26, https://doi.org/10.1007/s11249.019.1138.y. Art. no.
[28] H. Guo, P. Iglesias, Tribological behavior of ammonium-based protic ionic liquid as lubricant additive, Friction 9 (2021) 169–178, https://doi.org/10.1007/s40544.020.0378.z.
[29] T. Espinosa, J. Sanes, A.E. Jimenez, M.D. Bermudez, Protic ammonium carboxylate ionic liquid lubricants of OFHC copper, Wear 303 (2013) 495–509, https://doi.org/10.1016/j.wear.2013.03.041.
[30] H. Guo, J.R. Pang, A.R. Adukure, P. Iglesias, Influence of hydrogen bonding and ionicity of protic ionic liquids on lubricating steel-steel and steel-aluminum contacts: potential ecofriendly lubricants and additives, Tribol. Lett. 68 (2020) 114, https://doi.org/10.1007/s11249.020.01354.1.
[31] R. Kreivaitis, M. Gumbyte, A. Kupcinskas, K. Kazancev, T.N. Ta, J.H. Horng, Investigation of tribological properties of two protic ionic liquids as additives in water for steel-steel and alumina-steel contacts, Wear 456 (2020) 203390, https://doi.org/10.1016/j.wear.2020.203390. Art. no.
[32] M.D. Avilés, F.J. Carrión, J. Sanes, M.D. Bermúdez, Effects of protic ionic liquid crystal additives on the water-lubricated sliding wear and friction of sapphire against stainless steel, Wear 408–409 (2018) 56–64, https://doi.org/10.1016/j.wear.2018.04.015.
[33] F.J. Carrión, M.D. Avilés, K. Nakano, C. Tadokoro, T. Nagamine, M.D. Bermúdez, Diprotic ammonium palmitate ionic liquid crystal and nanodiamonds in aqueous lubrication. Film thickness and influence of sliding speed, Wear 418–419 (2019) 241–252, https://doi.org/10.1016/j.wear.2018.12.011.
[34] M.D. Aviles, V.D. Cao, C. Sanchez, J. Arias-Pardilla, F.J. Carrion-Vilches, J. Sanes, A.L. Kjoniksen, M.D. Bermudez, R. Pamies, Effect of temperature on the rheological behavior of a new aqueous liquid crystal biolubricant, J. Mol. Liquids 301 (2020) 112406, https://doi.org/10.1016/j.molliq.2019.112406.
[35] M.D. Avilés, V.D. Cao, C. Sánchez, J. Arias-Pardilla, F.J. Carrión-Vilches, J. Sanes, A.L. Kjoniksen, M.D. Bermúdez, R. Pamies, Corrigendum to “Effect of temperature on the rheological behavior of a new aqueous liquid crystal bio-lubricant, [J. Mol. Liquids 301 (2020) 112406, https://doi.org/10.1016/j.molliq.2020.112645. J. Mol. Liquids 2020; 303:112645.
[36] M.D. Avilés, R. Pamies, J. Sanes, F.J. Carrión, M.D. Bermúdez, Fatty-acid derived ionic liquid lubricant. Protic ionic liquid crystals as protic ionic liquid additives, Coatings 9 (2019) 71, https://doi.org/10.3390/coatings9110710.
[37] C.J. Reeves, A.K. Kasar, P.I. Menezes, Tribological performance of environmentally friendly ionic liquids for high-temperature applications, J. Cleaner Prod. 279 (2021) 123666, https://doi.org/10.1016/j.jclepro.2020.123666.
[38] G.W. Huang, Q.L. Yu, M.R. Cai, F. Zhou, W.M. Liu, Investigation of the lubricity and antiwear behavior of guanidinium ionic liquids at high temperatures, Tribol. Int. 114 (2017) 65–76, https://doi.org/10.1016/j.triboint.2017.04.010.
[39] P. Iglesias, M.D. Bermudez, F.J. Carrion, G. Martinez-Nicolas, Friction and wear of aluminium-steel contacts lubricated with ordered fluids-neuthttpsral and ionic liquid crystals as oil additives, Wear 256 (2004) 386–392, https://doi.org/10.1016/S0043-1648(03)00442-3.
[40] M.D. Avilés, C. Sánchez, R. Pamies, J. Sanes, M.D. Bermúdez, Ionic liquid crystals in tribology, Lubricants 7 (2019), https://doi.org/10.3390/lubricants7090072 article number 72.
[41] K. Kaneko, M. Akamatsu, K. Sakai, H. Sakai, Adsorption of hydrophilic amine-based protic ionic liquids on iron-based substrates, J. Oleo Sci. 70 (2021) 333–339, https://doi.org/10.5650/jos.ess20279.
[42] J.A. Williams, Engineering Tribology, Oxford University Press, 1994, ISBN 0 19 856503 8.
[43] J. Qu, J.J. Truhan, An efficient method for accurately determining wear volumes of sliders with non-flat wear scars and compound curvatures, Wear 261 (2008) 848–855, https://doi.org/10.1016/j.wear.2006.01.009.
[44] J.B. Luo, X. Zhou, Superlubricitive engineering-Future industry nearly getting rid of wear and frictional energy consumption, Friction 8 (2020) 643–665, https://doi.org/10.1007/s40544.020.0393.0.
[45] J. Li, C. Zhang, M. Deng, J. Luo, Investigations of the superlubricity of sapphire against ruby under phosphoric acid lubrication, Friction 2 (2014) 164–172, https://doi.org/10.1007/s40544.014.0050.6.
[46] S. Marcelin, N. Pebere, Electrochemical characterization of a martensitic stainless steel in a neutral chloride solution, Electrochim. Acta 87 (2013) 32–40, https://doi.org/10.1016/j.electacta.2012.09.011.
[47] N. Rivera, D. Blanco, J.L. Viesca, A. Fernandez-Gonzalez, R. Gonzalez, A.H. Battez, Tribological performance of three fatty acid anion-based ionic liquids (FAILs) used as lubricant additive, J. Mol. Liquids 296 (2019), https://doi.org/10.1016/j.molliq.2019.111881. Article number 111881.
[48] P.N. Bodganovich, D.V. Tkachuk, Temperature distribution over contact area and “hot spots” in rubbing solid contact, Tribol. Int. 39 (2006) 1355–1360, https://doi.org/10.1016/j.triboint.2005.10.008.